THE UNIVERSITY OF MICHIGAN

COLLEGE OF ENGINEERING

DEPARTMENT OF ELECTRICAL ENGINEERING

Radiation Laboratory

VOR PARASITIC LOOP COUNTERPOISE SYSTEM

Interim Report No. 2 (1 October 1967 - 31 January 1968)

By

Dipak L. Sengupta and Joseph E. Ferris

15 February 1968

Contract FA 67 WA-1753, Project 330-004-05N
Contract Monitor: Mr. Merle Mayner, IM-762

8905-2-Q = RL-2188

Contract With: Federal Aviation Administration
Radar and Navaids Section
800 Independence Avenue, SE
Washington, DC 20553

Administered through:
OFFICE OF RESEARCH ADMINISTRATION • ANN ARBOR

I INTRODUCTION

This is the Second Interim Report on Contract FA 67 WA-1753, Project 330-004-05N "VOR Parasitic Loop Counterpoise System" and covers the period 1 October 1967 to 31 January 1968.

During this period we have carried out theoretical and experimental investigations of the radiation characteristics of thw VOR Parasitic Loop Counterpoise System. Some of the results of the study are reported briefly below. Details of the theoretical analysis and critical discussion of the experimental results will be reported in the forthcoming Final Report.

II THEORETICAL STUDY

In this section we discuss briefly the procedure used to obtain a theoretical expression for the radiation field produced by a parasitic loop counterpoise antenna. Discussion of the preliminary theoretical analysis of the radiation properties of such an antenna system was reported earlier (Sengupta, 1967a, b) .

The VOR parasitic loop counterpoise system is shown schematically in Fig. 1. The Alford loop is the dirven element. It is assumed that the parasitic loop is made of conducting wire of radius b . All other parameters of the system are as shown in the figure.

The principle of the analysis is as follows. At first, the current induced in the parasitic loop due to the field produced by the Alford loop above the counterpoise is determined. The radiation fields produced by the Alford loop and the parasitic loop each in the presence of the counterpoise are evaluated separately. The two fields are then superposed to obtain the expression for the radiation field produced by the complete system. The basic steps involved in the development of the theory are described in the following sections.

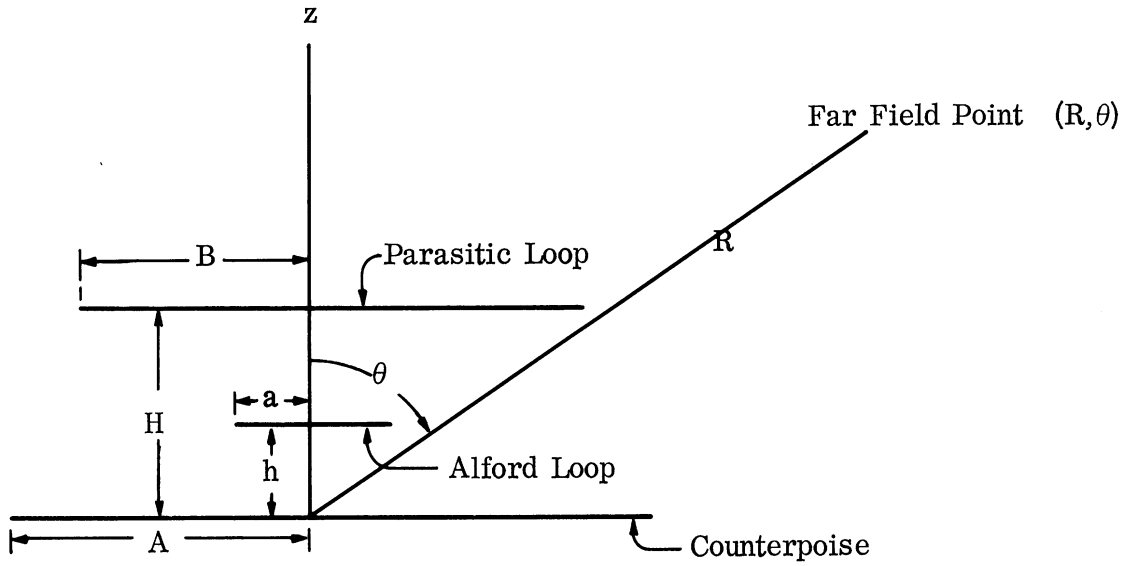

FIG. 1: GEOMETRIC REPRESENTATION OF THE VOR PARASITIC LOOP COUNTERPOISE SYSTEM.

2.1 Current Induced in the Parasitic Loop

The first step in the analysis is to obtain an expression for the current induced in the parasitic loop. From the symmetry of the system and also the nature of the incident field the current in the parasitic loop is assumed to be constant and of the following form:

$$\vec{I}_p = \hat{i}_\phi I_{p_o} e^{-i\omega t} , \tag{1}$$

where $\hat{i}_\phi$ is the unit vector in the ϕ direction and ω is the angular frequency of operation.

In finding I_{p_o} it is assumed that the current at any point in the parasitic loop is equal to that induced by a longitudinally polarized (the electric field is parallel to the axis) plane electromagnetic wave incident normally on a conducting cylinder of radius b and of infinite length. This is a reasonable assumption as long as $kB \gg 1$. Using the well-known results (Van Bladel, 1964) of the scattering of plane electromagnetic waves by an infinite cylinder it can be shown that

$$I_{p_o} = \frac{2\pi}{i\eta_o kP} E_\phi^{inc} , \tag{2}$$

where

η_o = intrinsic impedance of free space

$k = 2\pi/\lambda$ = propagation constant of free space

$P = 0.577 + \ell n \left(\frac{kb}{2}\right) - i\,\pi/2$

E_ϕ^{inc} is the field produced by the Alford loop and counterpoise at the position of the parasite.

In obtaining Eq. (2) it has been assumed that $kb \ll 1$ which is true for the present case. Thus the evaluation of I_{p_o} is now reduced to the evaluation of E_ϕ^{inc} which is discussed below.

The incident field at the parasitic loop is obtained by applying the ideas of geometrical theory of diffraction. E_{ϕ}^{inc} at the point P (Fig. 2) may be assumed to be due to the following components:

(i) incident and reflected rays 1 and 2 originating from the phase center of the Alford loop (Fig. 2),

(ii) rays originating from the Alford loop and singly diffracted from the near and far edges of the counterpoise; rays 3 and 4 in Fig. 3,

(iii) a ray incident from the Alford loop and diffracted by the diametrically opposite region P' of the parasitic loop; ray 5 in Fig. 4,

(iv) a ray incident from the Alford loop, singly diffracted at P and reflected back to P by the counterpoise; ray 6 in Fig. 4.

There are other diffracted rays that can contribute to E_{ϕ}^{inc}. However, they will be of smaller order and for the present analysis are neglected. Physical considerations dictate that the contributions due to the incident and reflected components will be dominant. All the other contributions will be less than this. It is also anticipated that for $kH \gg 1$, all the diffracted components will contribute negligibly. This is the case which was considered in in our last Interim Report (Sengupta and Ferris, 1967). However, for small and moderate values of kH the diffracted ray contributions can no longer be neglected. Let us now write E_{ϕ}^{inc} in the following manner:

$$E_{\phi}^{inc} = E_{\phi}^{12} + E_{\phi}^{34} + E_{\phi}^{56} , \tag{3}$$

where the superscripts on the right hand side refer to the rays contributing to the field. The detailed steps involved in obtaining explicit expression for E_{ϕ}^{inc} will not be discussed here.

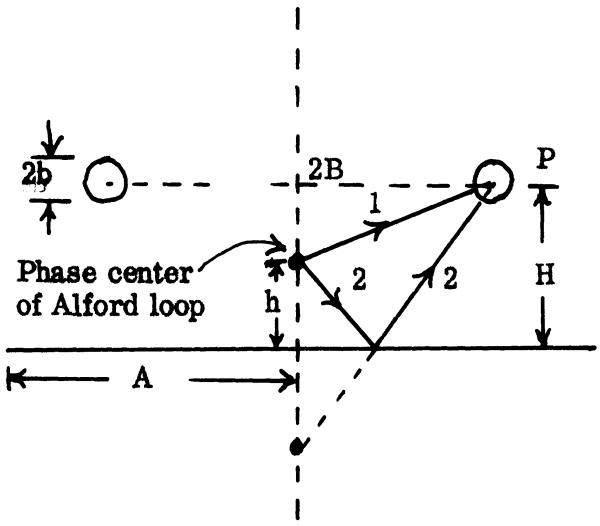

FIG. 2: DIAGRAM SHOWING THE EXCITATION OF THE PARASITIC LOOP DUE TO DIRECT AND REFLECTED RAYS.

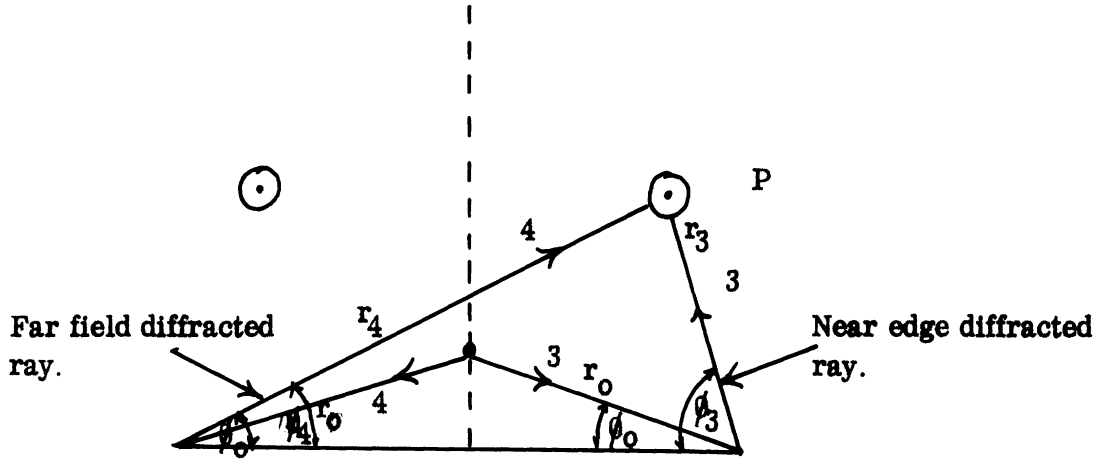

FIG. 3: DIAGRAM SHOWING THE EXCITATION OF THE PARASITIC LOOP DUE TO NEAR AND FAR EDGE DIFFRACTED RAYS.

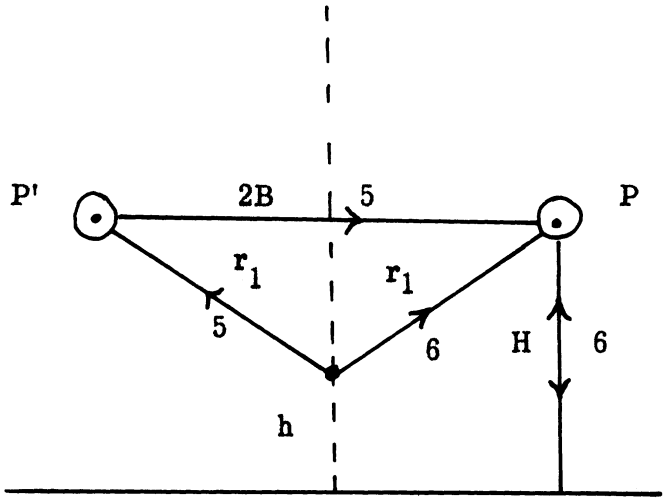

FIG. 4: DIAGRAM SHOWING THE EXCITATION OF THE PARASITIC LOOP DUE TO THE RAYS SINGLY DIFFRACTED BY THE PARASITIC LOOP.

After introducing Eq. (3) into (2), I_{p_o} is obtained in terms of the Alford loop current I_o and the other physical parameters of the system. Following the same convention used in (3) we may write

$$I_{p_o} = I_{p_o}^{12} + I_{p_o}^{34} + I_{p_o}^{56} \quad . \tag{4}$$

It can be shown that the component currents in (4) are given by the following:

$$I_{p_o}^{12} = I_o \left(\frac{ka}{2}\right)^2 \frac{2\pi B}{ikp} \left[\frac{e^{ikr_1}}{r_1^2} - \frac{e^{ikr_2}}{r_2^2}\right] , \tag{5}$$

$$\left.\begin{aligned} r_1^2 &= B^2+(H-h)^2 \\ r_2^2 &= B^2+(H+h)^2 \end{aligned}\right\} , \tag{6}$$

$$\begin{aligned} I_{p_o}^{34} = I_o\left(\frac{ka}{2}\right)^2 \cdot \frac{\pi}{ikp} \frac{A}{r_0^2} e^{ikr_o} \cdot \frac{e^{-i3\frac{\pi}{4}}}{\sqrt{2}} \left(\frac{A}{B}\right)^{1/2} \\ \times \left[\left(\frac{1}{\pi kr_3}\right)^{1/2} e^{ikr_3} \left\{\sec\left(\frac{\phi_o-\phi_3}{2}\right) - \sec\left(\frac{\phi_o+\phi_3}{2}\right)\right\}\right. \\ \left. + i\left(\frac{1}{\pi kr_4}\right)^{1/2} e^{ikr_4} \left\{\sec\left(\frac{\phi_o-\phi_4}{2}\right) - \sec\left(\frac{\phi_o+\phi_4}{2}\right)\right\}\right] \end{aligned} \tag{7}$$

where the notations are explained in Fig. 3,

$$\begin{aligned} I_{p_o}^{56} = I_o\left(\frac{ka}{2}\right)^2 \cdot \frac{\pi^2(kB)}{p^2} \frac{e^{ikr_1}}{(kr_1)^2} \left[\frac{1}{\sqrt{3}} \left(\frac{1}{\pi kB}\right)^{1/2} e^{i(2kB-\pi/4)} - \right. \\ \left. - \left(\frac{1}{\pi kH}\right)^{1/2} e^{i(2kH-\pi/4)}\right] \quad . \end{aligned} \tag{8}$$

2.2 Determination of the Far Field

The far field produced by the parasitic loop counterpoise system with Alford loop current I_o and parasitic loop current I_{p_o} is now determined following the procedure discussed elsewhere (Sengupta, 1967a, b). The far field expression can be written formally as follows:

$$E_{\phi}^{s} \sim \eta_o I_o \left(\frac{ka}{2}\right)^2 \frac{e^{i(kR-\pi/4)}}{R} \; S(\theta) \; , \tag{9}$$

where

$$S(\theta) = S^{A}(\theta) + S_{12}^{P}(\theta) + S_{34}^{P}(\theta) + S_{56}^{P}(\theta) \; . \tag{10}$$

In Eq. (9), $S^{A}(\theta)$ is the free space complex far field pattern produced by the Alford loop above the counterpoise only; the last three terms in (9) constitute the complex far field produced by the parasitic loop carrying current I_{p_o} in the presence of the counterpoise. $S(\theta)$ is identified as the complex far field produced by the complete parasitic loop counterpoise system. All the terms in Eq. (10) are complicated functions of the parameters A, B, b, H and h and of the Fresnel integrals involving some of these parameters. The detailed derivations of these expressions will be discussed in the Final Report

2.3 Comparison Between Theory and Experiment

A measured pattern of the parasitic loop counterpoise system is shown in Fig. 6. In this particular arrangement, the parasitic loop is placed very close to the plane of of the Alford loop. This particular value of H is chosen to test the theory because it is in this range of H where the maximum disagreement between theory and experiment is anticipated. The theoretical pattern as given by $\left|S^{A}(\theta) + S_{12}^{P}(\theta)\right|$ is superposed in Fig. 5. As can be seen the agreement between the two is fairly well over most of the range θ, despite the fact that this pattern has been computed by neglecting all diffraction effects in the determination of the parasitic loop current. In order to improve the theory, the pattern is

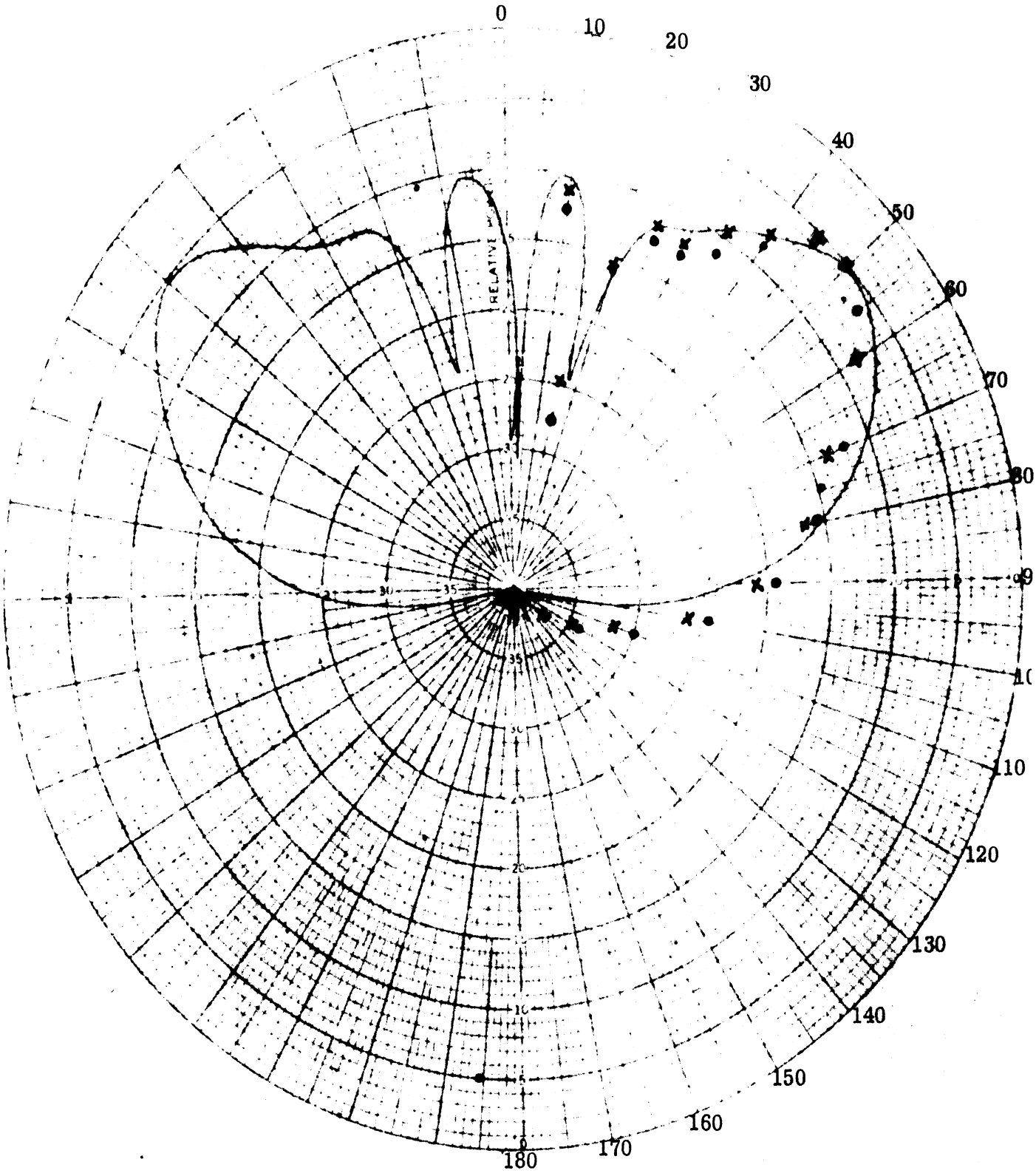

FIG. 5: FREE SPACE FAR FIELD PATTERN PRODUCED BY A LOOP COUNTERPOISE ANTENNA WITH ONE PARASITIC ELEMENT. kh=2.75, kH=3.75, kA=17.92, kb=0.15, kB=4π. —— Experimental, ••• $|S^{A}+S^{P}_{12}|$ Theoretical, ××× $|S^{A}+S^{P}_{12}+S^{P}_{56}|$ Theoretical.

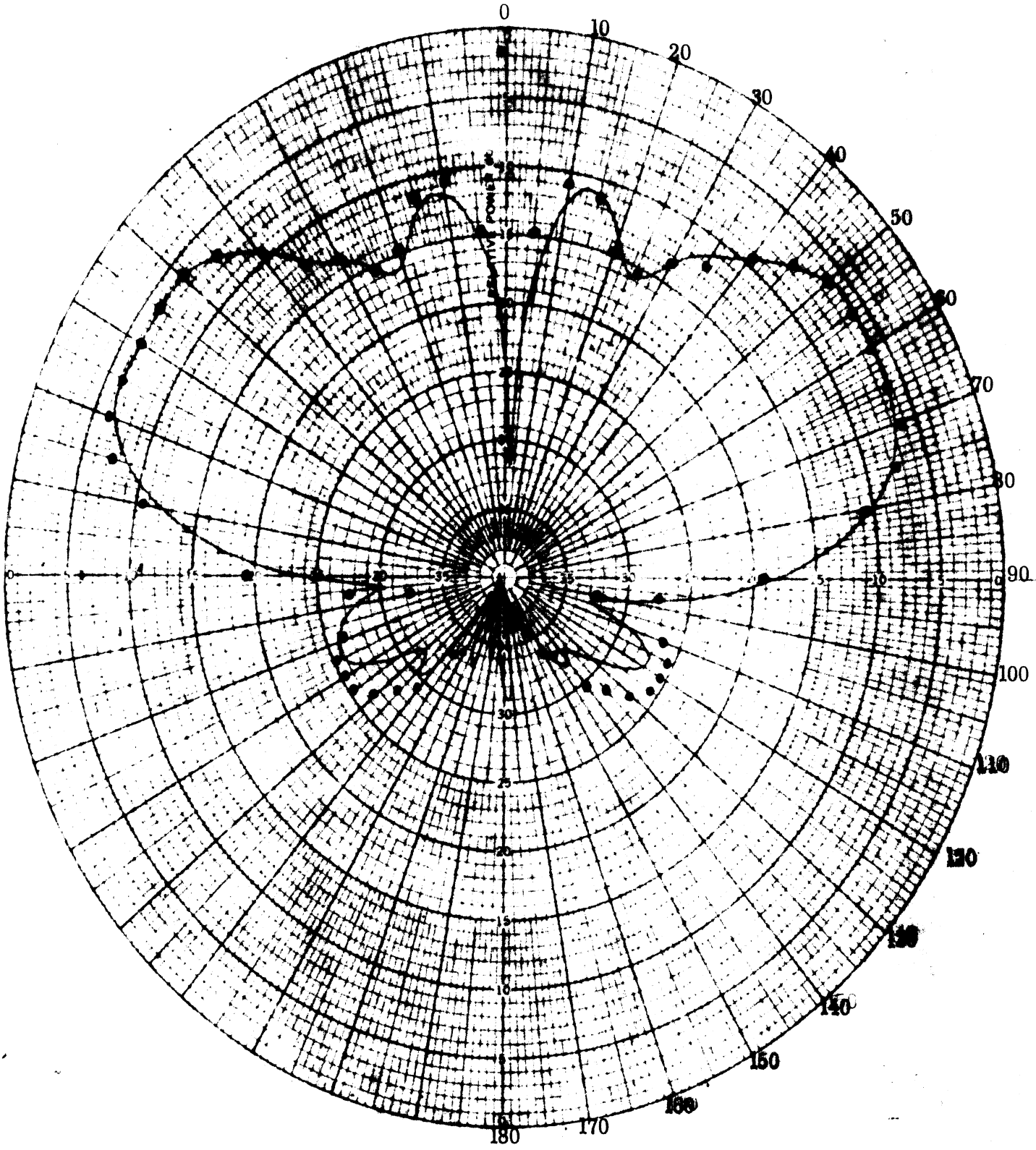

FIG. 6: FREE SPACE FAR FIELD PATTERN PRODUCED BY A LOOP COUNTERPOISE ANTENNA WITH ONE PARASITIC ELEMENT. kh=2.75, kH=11.78, kA=17.92, kb=0.15, kB=3π.
——— Experimental • • • Theoretical $\left| S^{A}+S^{P}_{12}+S^{P}_{56} \right|$.

then computed by taking into account the diffraction effects. It has been found by numerical computation that $|S_{34}(\theta)|$ is negligible compared to the other terms in Eq. (10) and hence it has been neglected for the present. The pattern as computed from $|S^{A}(\theta)+S^{P}_{12}(\theta)|$ is also shown in Fig. 5 for comparison. It can be seen that the corrected theory improves the agreement slightly. The present theory may be improved further by taking into account higher order diffraction terms in finding the current in the parasitic loop. It is anticipated that for larger values of H and B, the present theory should agree better than that shown in Fig. 5. This can be seen from Fig. 6 which shows the measured and theoretical patterns for the case kH= 11.78, kB= $.3\pi$, kb = 0.15. The agreement between theory and experiment is excellent in this case.

On the basis of the above it may be concluded that the theory developed for the loop counterpoise system is dependable and can be used for the optimization study of the pattern.

2.4 Numerical Results

Extensive patterns have been computed numerically by using Eq. (10). The pattern produced by the Alford loop above the ground plane ($S^{A}(\theta)$) has been computed for A = 10', 15', 20' and 26'. This has been done in order to study the effects of the counterpoise size on the pattern and to test the range of validity of the Alford loop counterpoise theory. Complete patterns of the parasitic loop counterpoise system have been computed for various combinations of the parameters as follows:

kH = 3.75, 4.00, 10.6(0.3)12,

kb = 0.15(0.5)0.35,

kB = $2\pi(0.25\pi)5\pi$.

In addition to the above, patterns have been computed for the 150' counterpoise system with the following parameters:

kh=2.75, kb = 0.15, kH = 3.75, kA = 51.69,

and kB = $3\pi(0.5\pi)15\pi$.

The numerical results are now currently analyzed and the results will be reported in the future.

2.5 Multiple Parasitic Loop System

As discussed before, using a single parasitic loop it is possible to obtain a minimum in the pattern at some angle below the horizon (see Fig. 6). However, the minimum is not deep enough to produce the desired field gradient at the horizon. To improve the field gradient we have done limited amount of study by using two parasitic loops placed parallel to each other and to the ground plane (Fig. 7). Theoretically it seems that this system is capable of producing a strong null below the horizon. Using two parasitic loops with dimensions $kH_1=3.75$, $kb=0.15$, $kB_1=4\pi$ and $kH_2=11.78$, $kb=0.15$ and $kB_2=3\pi$, a null was expected to appear in the direction 6^o below the horizon and of amplitude about 20 db below that at the horizon. The position as well as the amplitude of the null depend critically on slight variation of H_2. Figure 8 shows the measured pattern of a loop counterpoise system using two parasitic loops. It verified the theoretical predictions. Careful study of the pattern of Fig. 8 reveals that a minimum occurs at about $5^o.5$ below the horizon and its amplitude is about 20 db below that at the horizon. More details of this will be reported in the future. This aspect of the study is not complete. We feel strongly that this investigation should be pursued further because the two loop system appears to be capable of producing very strong field gradient at the horizon. The above field gradient of about 18 db/5^o is far better than any reported so far.

III EXPERIMENTAL STUDIES

The experimental investigation of the VOR system has continued employing a tenth scale Alford loop noted in the first Interim Report (Sengupta and Ferris 1967). A photograph of the Alford loop model is shown in Fig. 9. Experimental data has been collected (at a scale frequency of 1080 MHz) for an Alford loop located 4.8" above a 5'2" diameter counterpoise. The scale model of the VOR antenna mounted over the counterpoise is shown in Fig. 10. A typical rectangular plot of the elevation pattern of this system is presented in Fig. 11.

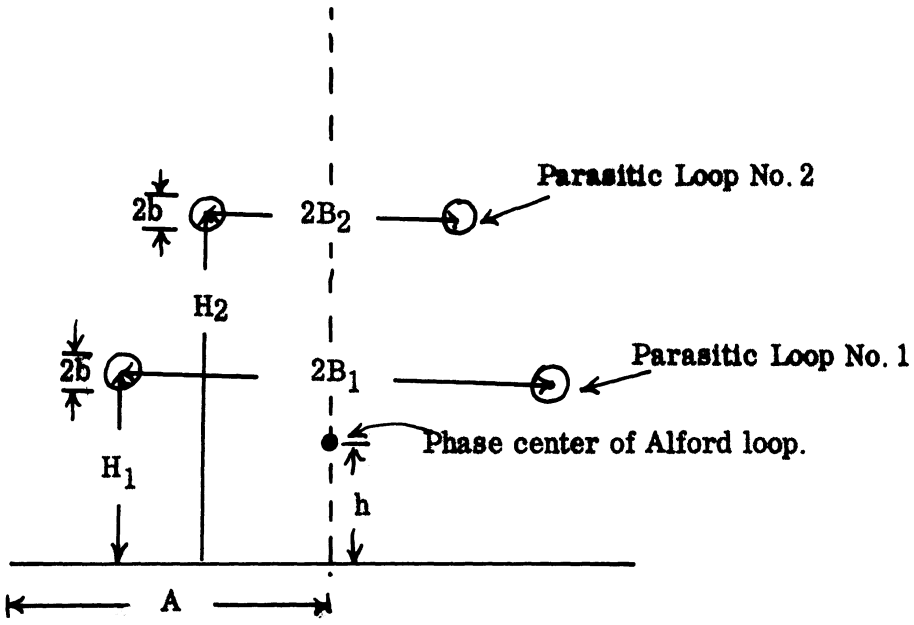

FIG. 7: DIAGRAM OF SYSTEM USING TWO PARASITIC LOOPS.

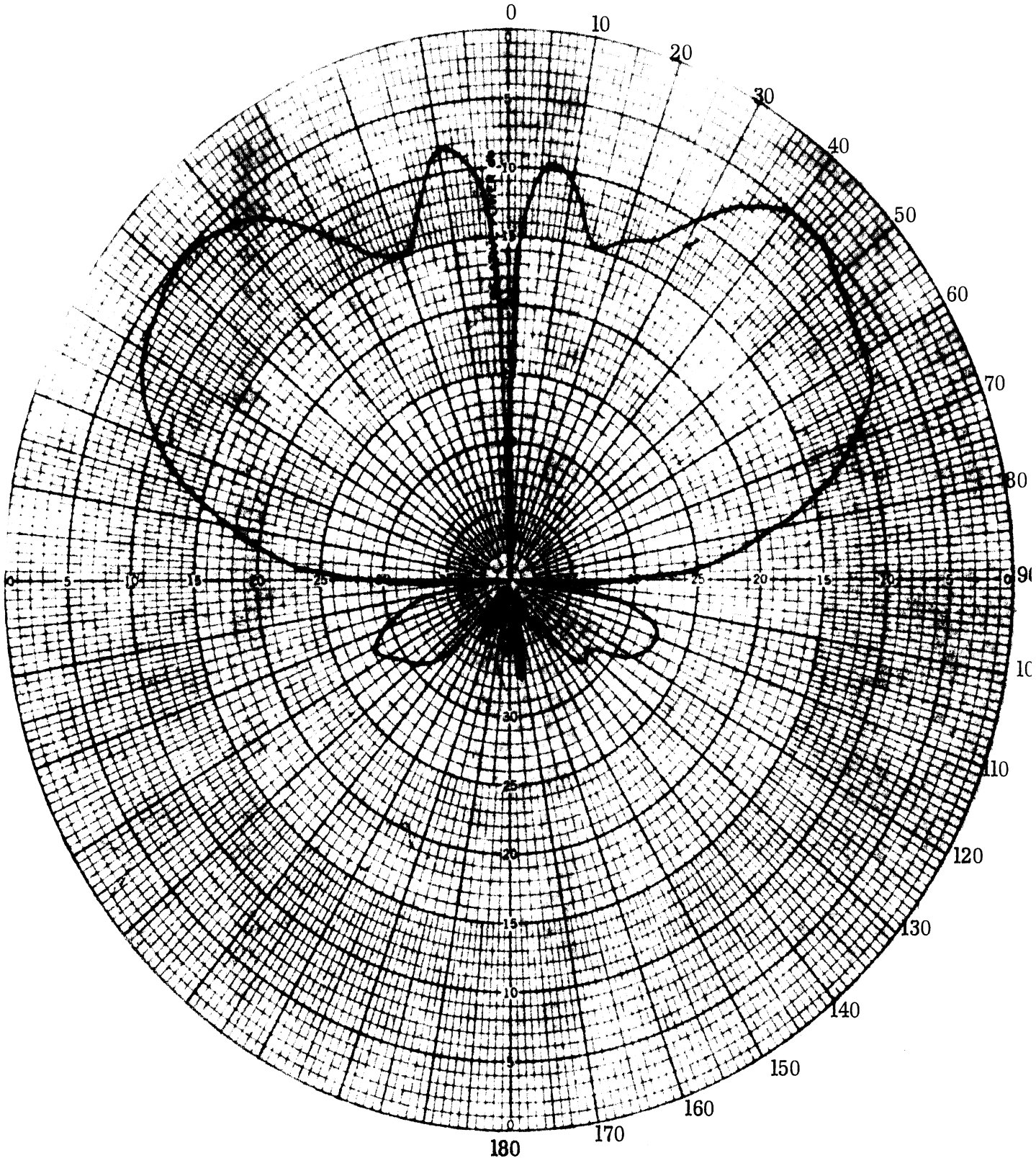

FIG. 8: MEASURED FAR FIELD PATTERN OF LOOP COUNTERPOISE ANTENNA WITH TWO PARASITIC ELEMENTS.
$w_1=2_2=1''$, $H_1=6.5''$, $H_2=18.5''$, $2B_1=43\ 1/2''$, $2B_2=35\ 3/4''$, f=1080 MHz.

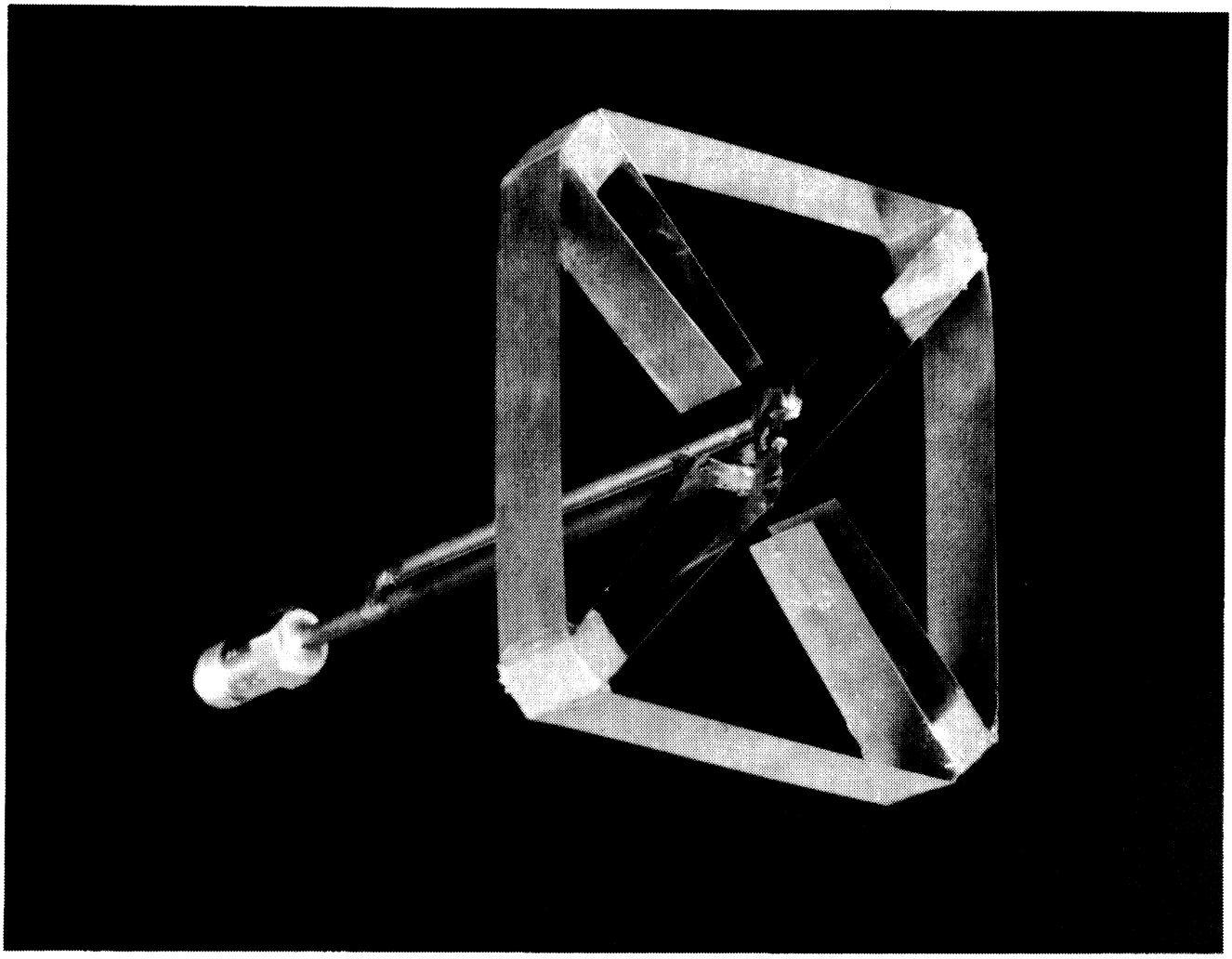

FIG. 9: Alford Loop 10th Scale Model (Frequency = 1080 MHz)

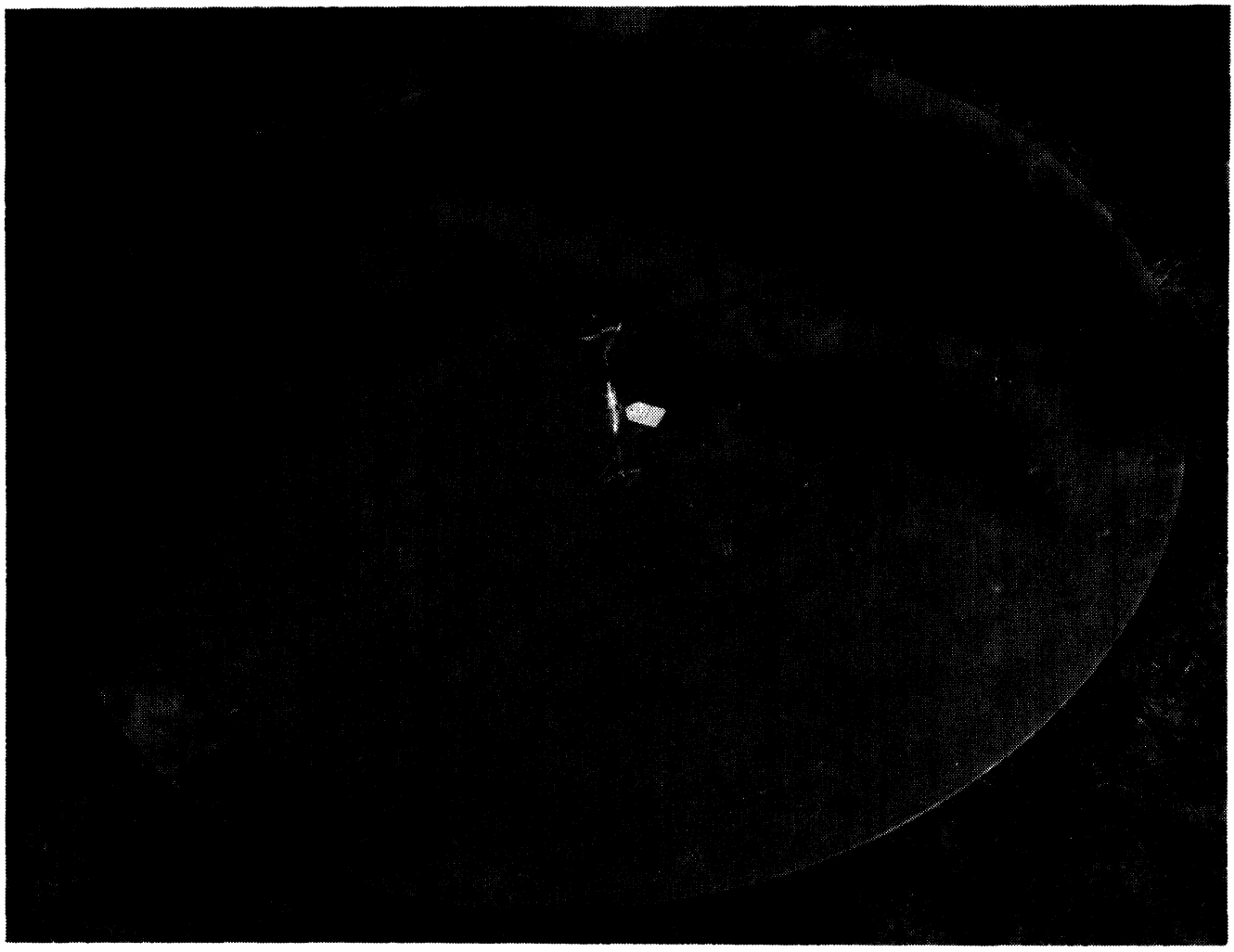

FIG. 10: TENTH SCALE ALFORD LOOP MOUNTED OVER 5'2" COUNTER-POISE.

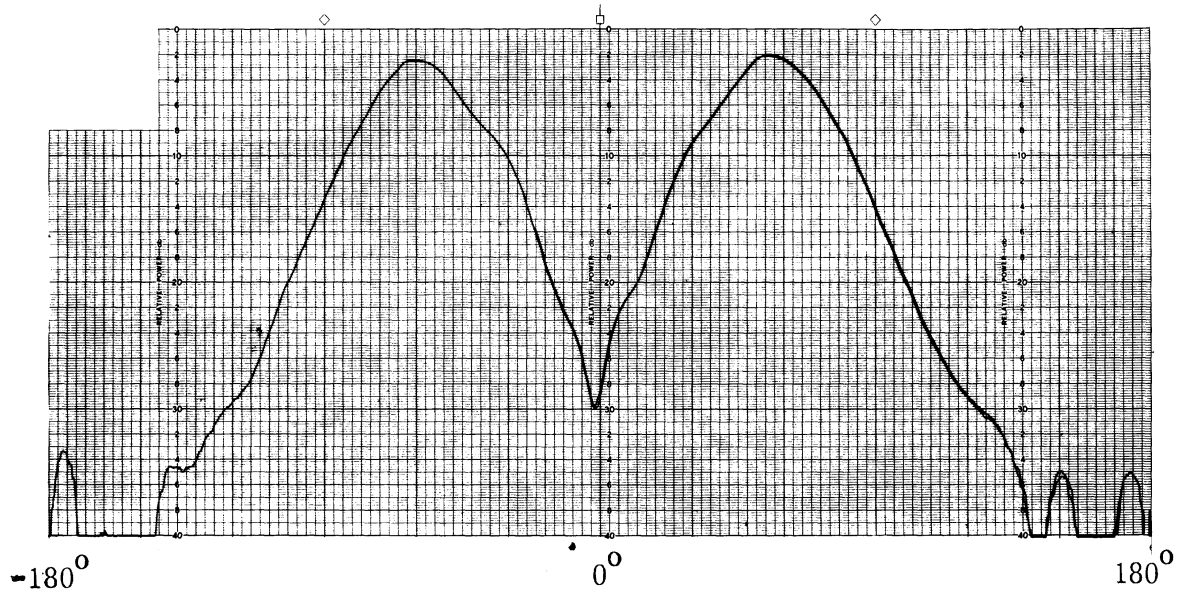

FIG. 11: MEASURED FREE SPACE PATTERN OF ALFORD LOOP MOUNTED 4.8" ABOVE 5'2" CIRCULAR GROUND PLANE (Freq. = 1080 MHz).

As part of our investigation into the feasibility of employing a parasitic element to improve the radiation characteristics of the Alford loop counterpoise system, several configurations were considered (a typical set-up is shown in Fig. 12). Table I lists the various configurations that have been investigated during this interim. The parasitic loops are made of strips of copper. Two specific loop widths have been considured; 1" and 2" . With the 1" wide parasitic loop element, three configurations were investigated. For the first configuration, the diameter of the parasitic element was varied from one wavelength to five wavelength in half-wavelength increments, and the spacing between the parasitic element and the counterpoise was varied from 2.5" to 20.5" in 2-inch increments. Data collected from this experiment showed some encouraging results as shown in Fig. 13, which shows a field gradient of about 7db/5^{o} below the horizon.

The seond configuration employed two 1" parasitic elements. For this experiment, the parasitic elements were located co-planar above the ground plane (i.e. $H_1=H_2$ in Fig. 7). The spacing between the co-planar loops and the counterpoise was varied from 4.5" to 20.5" in two-inch increments. At each level the diameter of one loop ($2B_1$) was held fixed while the diameter of the second parasitic element ($2B_2$) was varied from 1 - 3.5λ , in .5λ increments. Then the diameter of $2B_1$ was increased by a half wavelength, and the diameter of $2B_2$ was again varied through the range noted above. This continued until data for all combinations of $2B_1$ and $2B_2$ had been collected for the 4.5" spacing. This procedure was then repeated at each level noted above until a complete set of data had been collected as shown in Table I. Although the results of this study produced some encouraging patterns (Fig. 14) the field gradient was not improved as compared with the single parasitic loop case shown in Fig. 13.

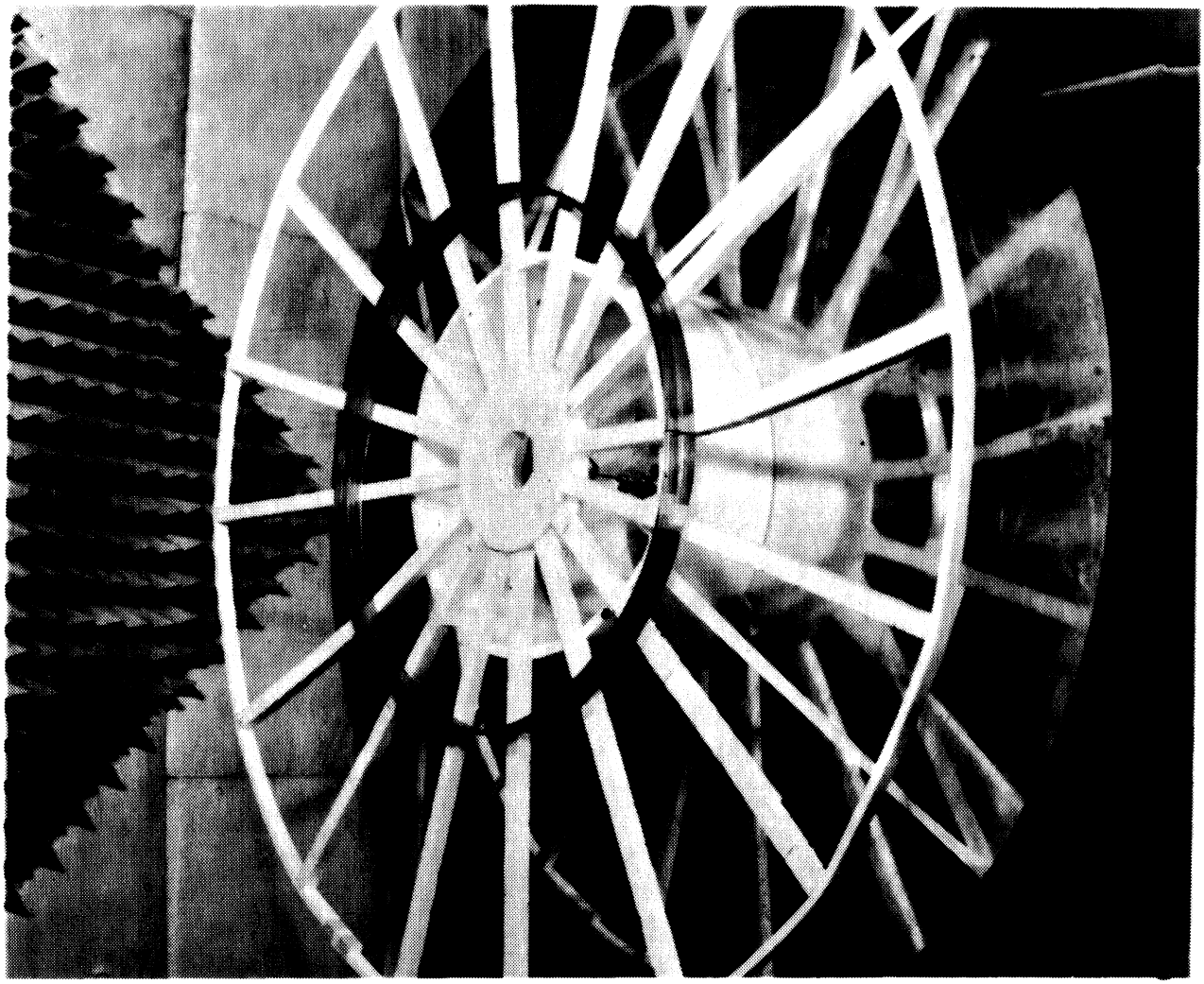

FIG. 12: TYPICAL SETUP TO INVESTIGATE PARASITIC LOOP FEASIBILITY (Freq. = 1080 MHz).

TABLE I: ALFORD LOOP AND PARASITIC ELEMENT CONFIGURATION
(Frequency = 1080 MHz)

One 1" loop: 5'2" Ground Plane:			
H	2.5"	20.5"	2" increments
2B	1λ	5λ	0.5λ increments
Two '" Loops 5'2" Ground Plane:			
$H_1=H_2$	4.5"	20.5"	2" increments
$2B_1$	1λ	3.5λ	0.5λ increments
$2B_2$	1λ	3.5λ	0.5λ increments
Four 1" Loops, 5'2" Ground Plane;			
H	2.5"	20.5"	2" increments
$2B_1$	1λ		
$2B_2$	2λ		
2B	3λ		
2B	4λ		
One 2" Loop, 5'2" Ground Plane:			
H	5.0"	9.0"	2" increments
2B	1λ	5λ	0.5λ increments
One 2" Loop, 5'2" Ground Plane: H=7", 2B = 27.3":			
1080 MHz - 1180 MHz			10 MHz increments
One 2" Loop, 2' Ground Plane:			
H	7"		
2B	1λ	5λ	0.5λ increments
One 2" Loop, 3' Ground Plane:			
H	7"		
2B	1λ	5λ	0.5λ increments
One 2" Loop, 4' Ground Plane:			
H	7"		
2B	1λ	5λ	0.5λ increments
Two 2" Loops, 5'2" Ground Plane:			
H_1	7"		
H_2	11"	21"	2" increments
$2B=2B_2$	$\approx$ 27"		

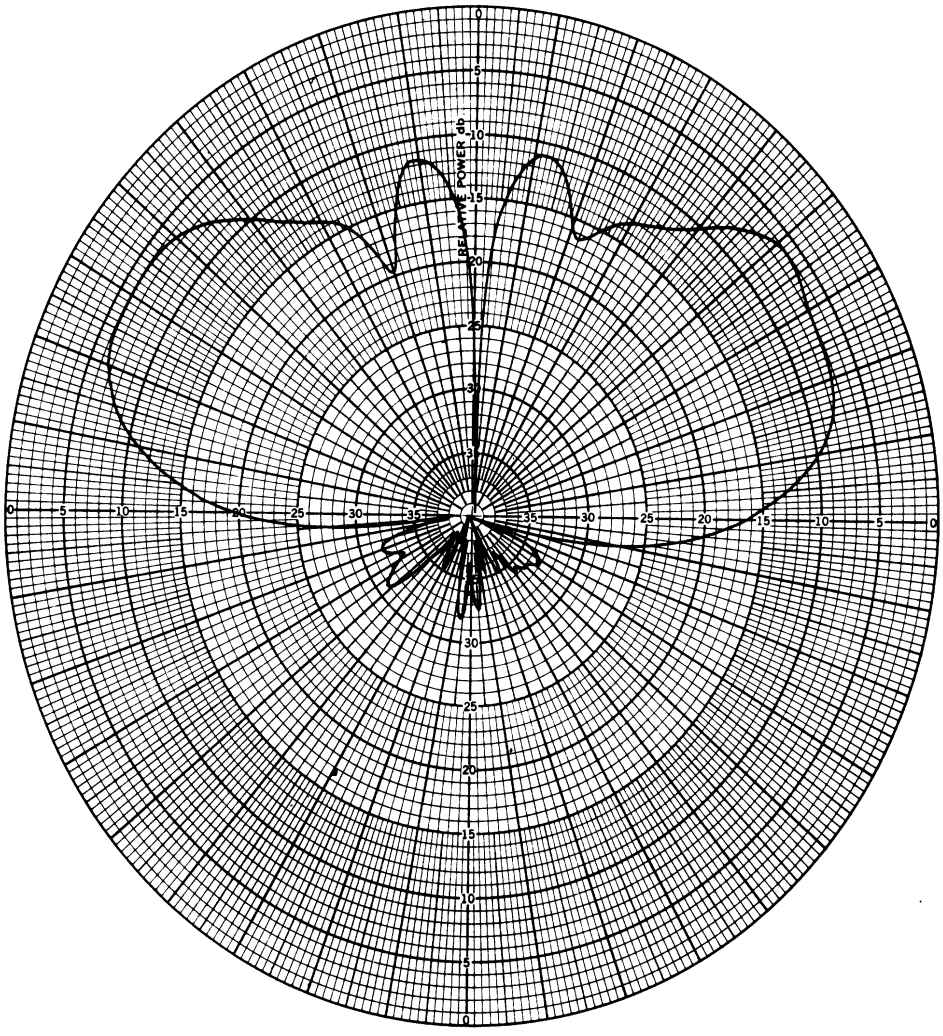

FIG. 13. MEASURED FREE SPACE PATTERN OF LOOP COUNTERPOISE ANTENNA WITH ONE PARASITIC ELEMENT.
w=0.09λ, 2B=3.0λ, H=1.95λ, Freq. = 1080 MHz.

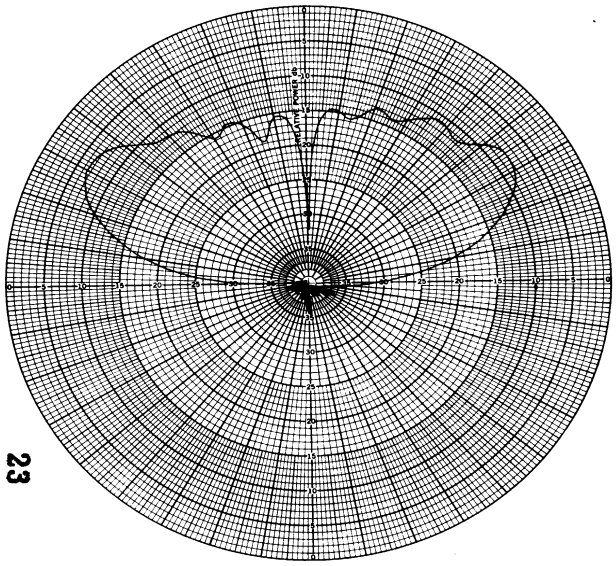

a.

$w = 0.09\lambda$; $2B_1 = 2\lambda$;

$2B_2 = 3.5\lambda$; $H_1 = H_2 = 0.06\lambda$

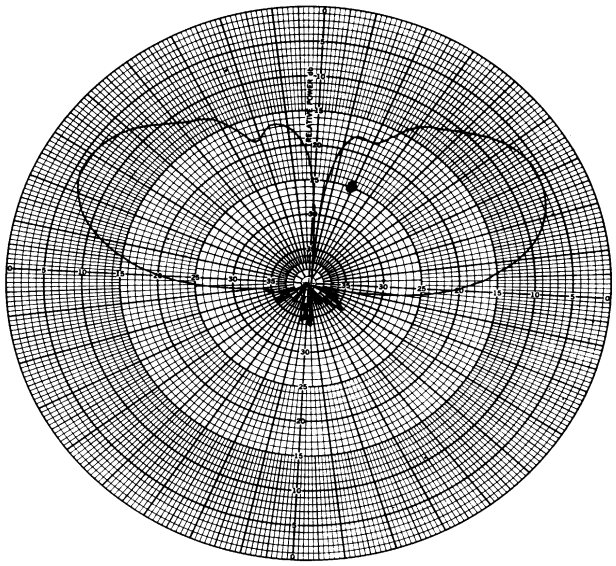

b.

$w = 0.09\lambda$; $2B_1 = 2\lambda$;

$2B_2 = 1.5\lambda$; $H_1 = H_2 = 1.7\lambda$

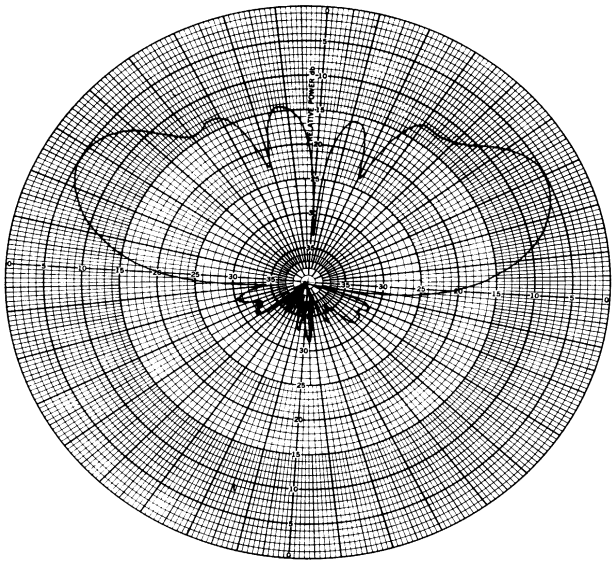

c.

$w = 0.09\lambda$; $2B_1 = 2\lambda$;

$2B_2 = 2.5\lambda$; $H_1 = H_2 = 1.7\lambda$

FIG. 14: MEASURED PATTERNS OF LOOP COUNTERPOISE ANTENNA WITH TWO CO-PLANAR PARASITIC ELEMENTS. (Freq. 1080 MHz).

A third configuration employing the 1" loop consisted of four loops arrayed in a co-planar configuration. The diameters of the loops were fixed as follows: 1λ, 2λ, 3λ and 4λ . Pattern data was collected for several co-planar levels above the counterpoise (from 2.5" to 20.5" in 2" increments). The results of this test were not encouraging since they did not exhibit desirable radiation characteristics for a VOR station. Perhaps this investigation should be continued with the spacing between elements and heights above the counterpoise varied in several different combinations. However, because of the lack of time only this initial investigation into the feasibility of employing multiple loops with the Alford loop to control the far field radiation patterns has been performed.

Data collected for the 2" loop configuration was obtained for three configurations. These were a single loop, a double loop system, and varying the ground plane size.

The data collected for the 1" loop was most encouraging when the parasitic element was located from 5 to 9 inches above the counterpoise. Therefore, employing a 2" loop, data was obtained with the loop spaced 5" - 9" above the counterpoise with the spacing being varied in 2" increments. Again the loop diameter was varied from 1λ - 5λ in 0.5λ increments. This data exhibited some encouraging results and a typical pattern for the loop 2.5λ in diameter, located 7" below the counterpoise is shown in rectangular form in Figs. 15a, b. It is to be noted that Fig. 15b was recorded by expanding (20 db) the lower portion of the data shown in Fig. 15a. Because of the encouraging data shown in this figure, additional data was collected for the configuration in the 1080 - 1180 MHz frequency range in 10 MHz increments. In general the data was similar to that of Fig. 15a, b., however the null at approximately 30^{o} tended to become more pronounced but did not seem to be objectionable.

The second configuration employed two 2" parasitic elements. These two elements were positioned co-linearly above the counterpoise. By this it is meant that both loops had the same diameter with one loop located a fixed distance of 7" above the counterpoise and the spacing of the second loop above the counterpoise was varied 11" - 21" in 2" increments. Results of this data were encouraging and a typical pattern is shown in Fig. 16. The field gradient

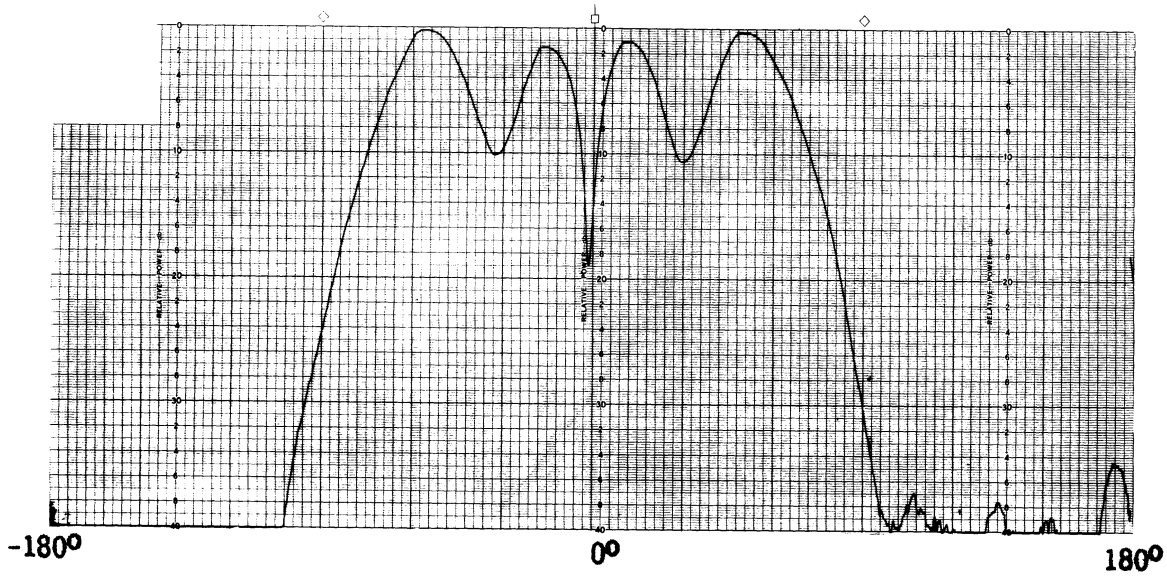

FIG. 15a: MEASURED FAR FIELD PATTERN OF LOOP COUNTERPOISE ANTENNA WITH ONE PARASITIC ELEMENT. w=0.17λ, 2B=2.5λ, H=0.64λ, Freq. =1080 MHz.

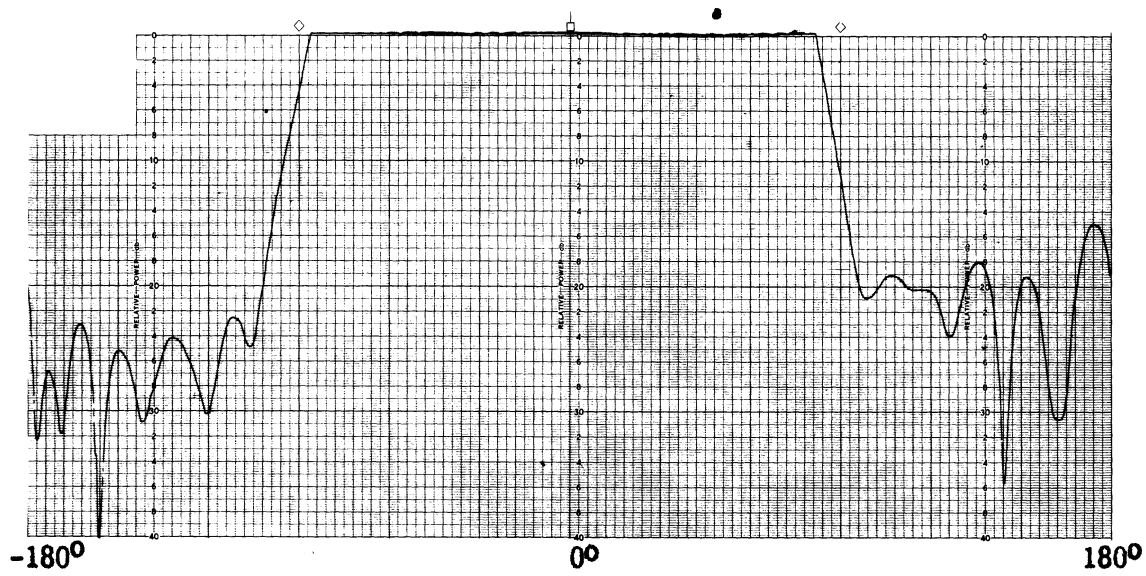

FIG. 15b: MEASURED FAR FIELD PATTERN OF LOOP COUNTERPOISE ANTENNA WITH ONE PARASITIC ELEMENT (AMPLIFIED 20 db). w=0.17λ, 2B=2.5λ, H=0.64λ, Freq. = 1080 MHz).

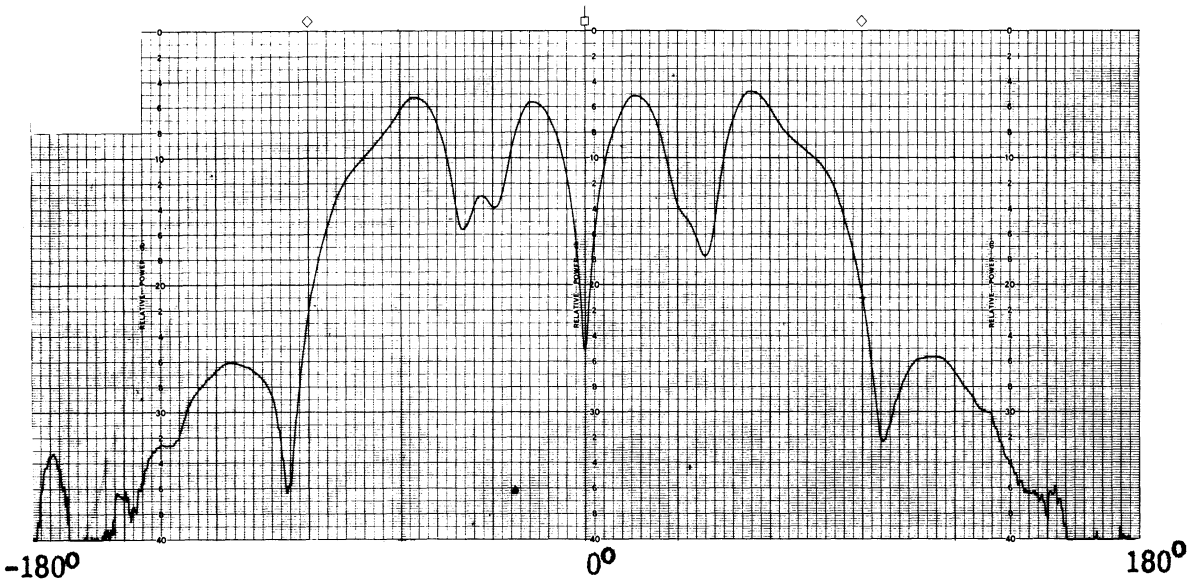

FIG. 16: MEASURED FAR FIELD PATTERN OF LOOP COUNTERPOISE ANTENNA WITH TWO CO-LINEAR PARASITIC ELEMENTS.
$w_1 = w_2 = 0.17\lambda$, $2B_1 = 2B_2 = 2.5\lambda$, $H_1 = 0.64\lambda$, $H_2 = 0.92\lambda$, Freq. = 1080 MHz.

obtained is about 11 db/5°. The two loop system discussed in Section II produced a better field gradient.

For the third configuration employing the 2" parasitic element, data was collected employing 2, 3 and 4-foot counterpoises. Data collected for the 2' through 4' counterpoise employed the 2" parasitic element positioned 7" above the counterpoise; its diameter was varied from 1λ - 5λ in 0.5λ increments. The results obtained are being analyzed.

Data collected during this period is being reduced and will be presented in a tabuled form in the Final Report. In this way one may obtain a better appreciation for the effect of employing parasitic elements with the Alford loop configuration.

IV EFFECT OF FLAT EARTH

A short theoretical analysis was made assuming the Alford loop counterpoise system located at various heights above the earth. For the purposes of this analysis, the earth was assumed to be flat and perfectly conducting. The height of the antenna system above the earth was varied 5' - 75' in five-foot increments. The results of this study are shown in Fig. 17 for a single Alford loop with no parasitic element, and Fig. 18 for an Alford loop with a single parasitic element having free space radiation characteristics shown in Fig. 15. The area of major interest in these patterns (Figs. 17-18) is the first four degrees above the horizon. One can see from Fig. 17 the strong influence of reflected energy, from radiation below the horizon, from a conventional Alford loop without a parasitic element. Further, it can be seen that the pattern is strongly affected as the height of the antenna above the earth is varied. However, when a parasitic element is added to the system, to effect a free space pattern similar to Fig. 15, we see from Fig. 18 that there is little influence on the pattern (in the presence of the earth) as the antenna is raised above the surface of the earth. From this data one may observe that the height above the earth that an Alford loop counterpoise system is located (with no parasitic element), is extremely critical.

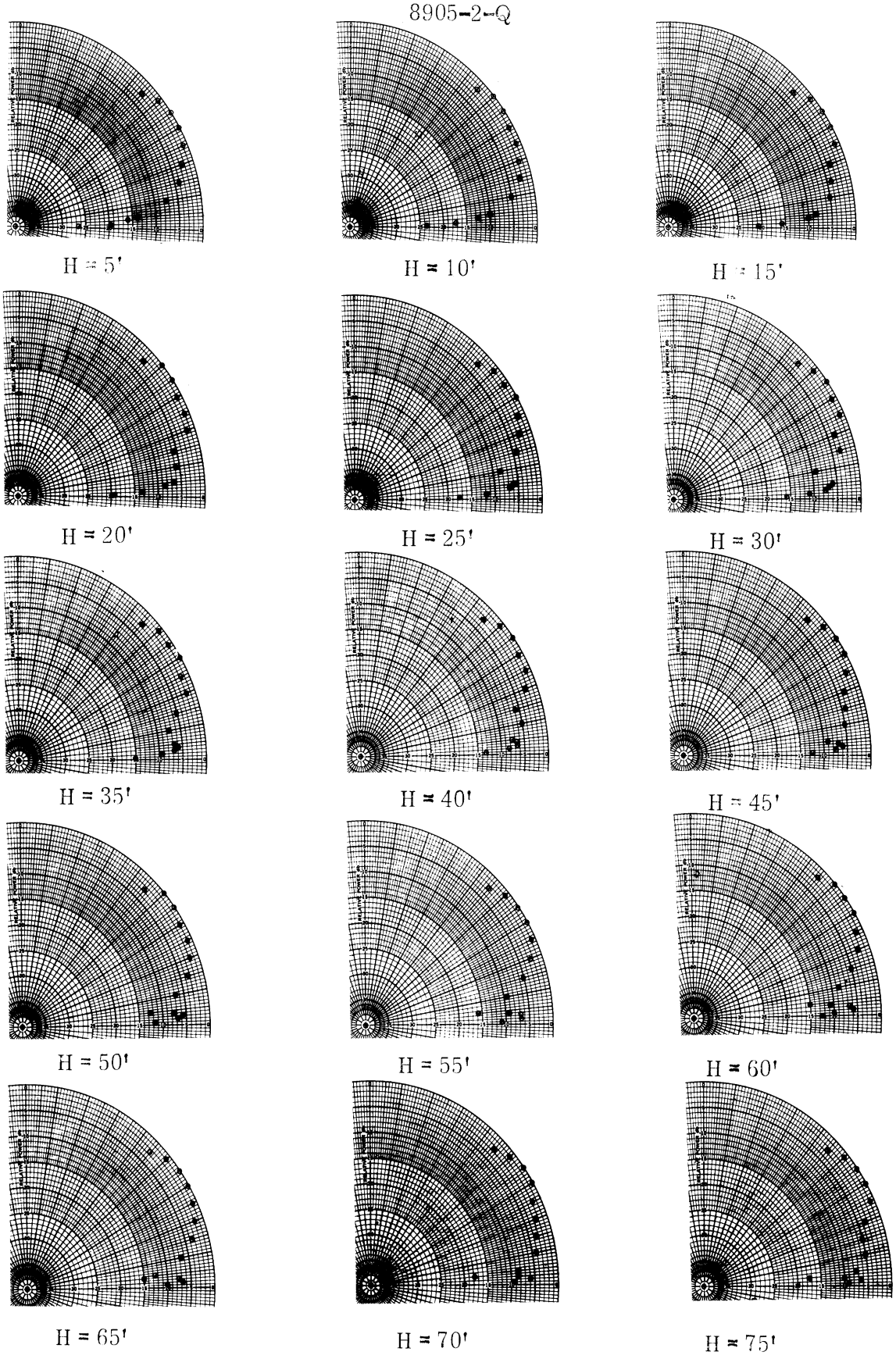

FIG. 17: THEORETICAL FAR FIELD PATTERN OF AN ALFORD LOOP - COUNTERPOISE SYSTEM LOCATED AT VARIOUS HEIGHTS ABOVE THE EARTH (H = 5' to 75').

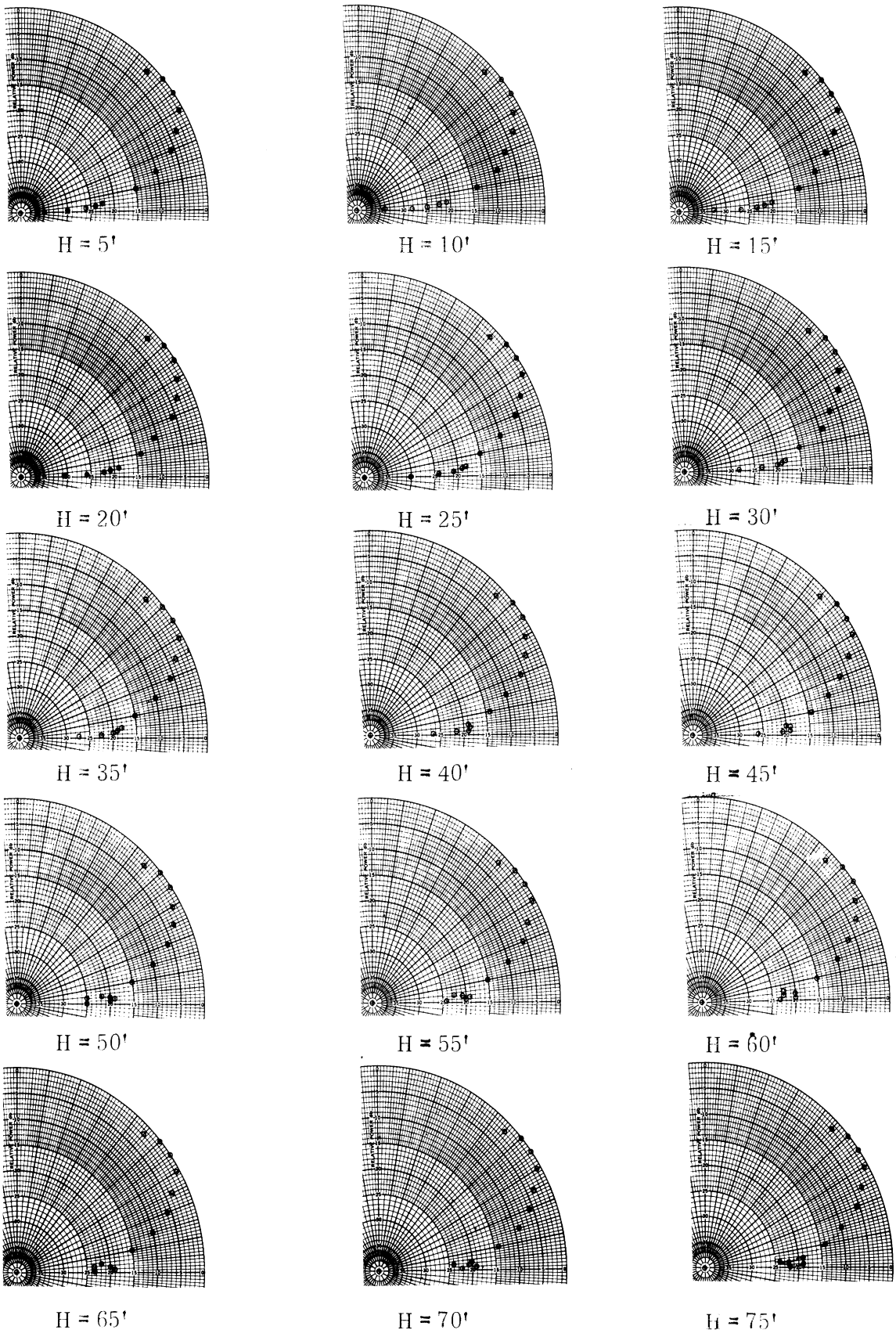

FIG. 18: THEORETICAL FAR FIELD PATTERN OF AN ALFORD LOOP PARASITIC COUNTERPOISE SYSTEM LOCATED VARIOUS HEIGHTS ABOVE THE EARTH (H = 5' to 75').

V CONCLUSIONS

A theory has been developed for the radiation field produced by a VOR antenna system consisting of an Alford loop and a large parasitic loop above a circular ground plane. For parameters within the range of approximation, the theory is found to agree very well with experiment. More study of the theory is necessary so that the loop parameters may be optimized. Although it has been found that one parasitic loop is capable of producing a minimum in the pattern in a direction a few degrees below the horizon, the minimum is not strong enough to give a field gradient better than about 7 db/5°. Two parasitic loop elements have produced a field gradient of 18 db/5° at the horizon while maintaining desirable pattern characteristics above the horizon.

VI RECOMMENDATIONS FOR FUTURE WORK

From our study it appears that a loop counterpoise system consisting of more than one parasitic loop is capable of fulfilling the pattern requirements for a VOR system. A field gradient of 18 db/5° below the horizon obtained with a two-parasitic loop system is much better than any reported from previous studies of the VOR system. Due to limitations of time we have not been able to complete the study of such multiple loop systems. We therefore strongly recommend that further study should be made along the following lines so that the full advantage of the multiple loop concept may be utilized in improving the present VOR antenna pattern characteristics:

1. Modify the present theory to explain the radiation field produced by a VOR antenna system using two or more parasitic loops.
2. Study theoretical expressions to optimize the different parameters.
3. Experimentally test the optimum models obtained above.
4. Obtain the proper dimensions of the multiple loop system for full scale testing.
5. Explore the concept of tuning the parasitic loops to adjust the pattern characteristics below the horizon.

VI REFERENCES

Sengupta, D. L. (1967a), "VOR Parasitic Loop Counterpoise System" Radiation Laboratory Memorandum 8905-502-M.

Sengupta, D. L. (1967b), "VOR Parasitic Loop Counterpoise System-II", Radiation Laboratory Memorandum 8905-504-M.

Sengupta, D. L. and J. E. Ferris (1967), "VOR Parasitic Loop Counterpoise System," Radiation Laboratory Interim Report No. 8905-1-Q.

Van Bladel, J. (1964), Electromagnetic Fields, McGraw-Hill Book Company, New York.